

6.4 Analyzing Vortex Winds in Radar Observed Tornadic Mesocyclones for Nowcast Applications

Qin Xu^{1*}, Li Wei² and Kang Nai²

¹NOAA/National Severe Storms Laboratory, Norman, Oklahoma

²Cooperative Institute for Mesoscale Meteorological Studies, University of Oklahoma

1. Introduction

Detecting and tracking mesocyclones from Doppler radial-velocity fields are very important for tornado-related severe weather warning operations, but the involved tasks often encounter enormous difficulties especially when mesocyclones are poorly resolved in the far radial ranges or confused with other signatures or data artifacts (such as noisy or improperly dealiased velocities) in radial-velocity fields. To overcome the encounter difficulties, various automated mesocyclone detection methods and algorithms have been developed by many investigators (Stumpf et al. 1998; Smith and Elmore 2004; Liu et al. 2007; Newman et al. 2013; Miller et al. 2013). These methods rely on the assumption that a mesocyclone is behaving as a Rankine vortex and identify it as an object with no attempt to diagnose the detailed vortex wind field. To diagnose the full storm wind field, Gao et al. (2013) adapted a real-time three-dimensional variational data assimilation (3DVar) system and showed the value of the wind field assimilated from multiple Doppler radar data. This 3DVar system compares favorably to the methods described above with regards to identifying storm-scale mid-level circulations, but the circulation may not be fully resolved due to the isotropic univariant background covariance used for each velocity component in the cost-function. It is possible to improve the mesocyclone wind analysis by formulating the background covariance with vortex-flow dependences in a moving frame following the mesocyclone. This approach is presented in this paper.

2. Vortex wind analysis

To resolve the mesocyclone, a new method is developed with the following three key components: (a) an algorithm for estimating the vortex center of the mesocyclone on a selected tilt of radar radial-velocity scan, (b) a vortex-flow-dependent background error correlation function formulated for the vortex wind analysis over the mesocyclone area on the selected tilt, and (c) the square root of the vortex-flow-dependent background error covariance matrix derived analytically to precondition the cost-function and thus enhance the computational efficiency. The method can be used as an additional (fourth) step of targeted fine-scale analysis after the third step is performed in the radar wind analysis system (RWAS, Xu et al. 2015a). It can be also used in a stand-alone fashion, as considered in this paper. In this case, it is necessary to estimate the environmental mean wind and use it as the background wind.

The detailed techniques in the three components are presented in the following subsections.

a. Estimating vortex center location

The mesocyclone area is identified as a by-product of the automated velocity dealiasing (see Appendix of Xu et al. 2013) on a selected tilt of radar low-elevation scan. The vortex center location is then estimated, also as a by-product of the automated velocity dealiasing, and is used here as the first guess. From this first guess, the vortex center location is further estimated in the mesocyclone area on the selected tilt by applying a two-step algorithm (see section 3a of Xu et al. 2015b) to the data field of dealiased radial-velocity observations, denoted by $v_r^o(r, \varphi)$, where r is the radial distance from the radar and φ is the radar beam azimuthal angle (positive for clockwise rotation from the y -coordinate pointing to the north) on the selected tilt. As by-products, the maximum tangential velocity V_M for the vortex and its radial distance R_M from the vortex center are estimated [see (3)-(4) of Xu et al. 2015b].

By assuming that the vortex moves mainly with the environment mean wind, the vortex center moving velocity estimated by the time change rate of vortex center location (on the same tilt from the previous to the current volume scan) will be used as the background wind, denoted by (u^b, v^b) . The radial component of (u^b, v^b) is given by

$$v_r^b = (u^b \sin \varphi + v^b \cos \varphi) \cos \theta,$$

where θ is the slope angle of radar beam relative to the Earth surface beneath the observation point, and the projection of the background vertical velocity is negligible for $\theta < 5^\circ$.

b. Vortex-flow-dependent background error covariance

The control variables used for the vortex wind analysis are the radial velocity, denoted by $V_R (> 0$ in the outward direction), and tangential velocity, denoted by $V_T (> 0$ in the counterclockwise direction), of the vortex part of the mesocyclone wind field. This vortex part is an incremental wind field, denoted by $(\Delta u, \Delta v)$, with respect to (u^b, v^b) . In the local (x, y) -coordinate system centered at the estimated vortex center, denote by (r_c, φ_c) , on the selected tilt, $(\Delta u, \Delta v)$ is related to (V_R, V_T) by

$$(\Delta u, \Delta v) = (V_R \cos \beta - V_T \sin \beta, V_R \sin \beta + V_T \cos \beta), \quad (1)$$

where $\beta \equiv \tan^{-1}(y/x)$. The radar observed radial component of $(\Delta u, \Delta v)$ can be modeled by

$$\begin{aligned} v_r &= (\Delta u \sin \varphi + \Delta v \cos \varphi) \cos \theta \\ &= [V_R \sin(\varphi + \beta) + V_T \cos(\varphi + \beta)] \cos \theta. \end{aligned} \quad (2)$$

Here, again, the projection of the vertical velocity w is neglected since θ is small ($< 5^\circ$) and w is not analyzed.

The cost-function for the vortex wind analysis has the following form:

* Corresponding author address: Qin Xu, National Severe Storms Laboratory, 120 David L. Boren Blvd., Norman, OK 73072-7326; E-mail: Qin.Xu@noaa.gov

$$J = \mathbf{a}^T \mathbf{B}^{-1} \mathbf{a} / 2 + (\mathbf{H} \mathbf{a} - \mathbf{d})^T \mathbf{O}^{-1} (\mathbf{H} \mathbf{a} - \mathbf{d}) / 2, \quad (3)$$

where $\mathbf{a} = (\mathbf{a}_R^T, \mathbf{a}_T^T)^T$, \mathbf{a}_R (or \mathbf{a}_T) is the state vector of V_R (or V_T), $(\)^T$ denotes the transpose of $(\)$, \mathbf{B} is the background error covariance matrix, \mathbf{O} is the observation error covariance matrix, \mathbf{H} is the observation operator expressed in (2), and \mathbf{d} is the innovation vector, that is, the state vector of $v_r^1 = v_r^0 - v_r^b$. The observation errors are assumed to be uncorrelated between different points, so $\mathbf{O} = \sigma_o^2 \mathbf{I}$, where σ_o^2 is the observation error variance and \mathbf{I} is the unit matrix in the observation space.

The random vector fields of background wind errors, denoted by $(\varepsilon_R, \varepsilon_T)$, are assumed to have zero mean, that is, $\langle \varepsilon_T \rangle = \langle \varepsilon_R \rangle = 0$ where $\langle \bullet \rangle$ denotes the statistical mean of (\bullet) . In addition, ε_R and ε_T are assumed to be not correlated and nearly homogeneous and isotropic in the following transformed polar coordinates:

$$\rho = l^{-1} \ln(1 + R/R_c), \quad (4a)$$

$$\phi = \beta / \Phi, \quad (4b)$$

where $R = |\mathbf{x}| = (x^2 + y^2)^{1/2}$, l and Φ are the scaling factors for ρ and ϕ , respectively, and R_c is the scaling factor for R and is set to $R_c = 1$ km according to the averaged horizontal resolution of radar radial-velocity observations.

The above assumed nearly homogeneity and isotropy imply that the covariance tensor function for $\boldsymbol{\varepsilon} = (\varepsilon_R, \varepsilon_T)^T$ has the following diagonal form:

$$\mathbf{B} = \langle \boldsymbol{\varepsilon}, \boldsymbol{\varepsilon}_j^T \rangle = (B_R, B_T)^{\text{diag}}, \quad (5a)$$

The two diagonal components of \mathbf{B} are modeled by

$$\begin{aligned} B_R &= \sigma_R^2 C(\rho_i, \rho_j, \phi_i - \phi_j), \\ B_T &= \sigma_T^2 C(\rho_i, \rho_j, \phi_i - \phi_j), \end{aligned} \quad (5b)$$

where σ_R (or σ_T) is the standard deviation of ε_R (or ε_T), and $C(\rho_i, \rho_j, \phi_i - \phi_j)$ is a pseudo-correlation function constructed by

$$C(\rho_i, \rho_j, \phi_i - \phi_j) = C_1(\rho_i, \rho_j) C_2(\phi_i - \phi_j), \quad (6a)$$

$$C_1(\rho_i, \rho_j) = \exp[-(\rho_i - \rho_j)^2 / 2] - \exp[-(\rho_i + \rho_j)^2 / 2], \quad (6b)$$

$$\begin{aligned} C_2(\phi_i - \phi_j) &= A_0^{-1} \sum_n \exp[-(\phi_i - \phi_j - 2n\pi/\Phi)^2 / 2] \\ &\approx \exp[-(\phi_i - \phi_j)^2 / 2] \text{ for } -\pi/\Phi \leq \phi_i - \phi_j \leq \pi/\Phi \text{ and } \Phi \leq 1, \end{aligned} \quad (6c)$$

where $A_0 = \sum_n \exp[-2(n\pi)^2 / \Phi^2] > 1$ to ensure $C_2(0) = 1$, and \sum_n denotes the summation over integer n from $-\infty$ to ∞ . For $\Phi \leq 1$, $A_0 \approx 1$ and the summation in (6c) can be truncated to a single term as shown in the last step of (6c).

In (6b), the Gaussian correlation function is modified by subtracting its mirror image obtained by mirror-reflecting the corrected point ρ_i (or ρ_j) with respect to $\rho = 0$, so $C_1(\rho_i, \rho_j)$ can have the desired property of $C_1(\rho_i, \rho_j) = 0$ for $\rho_i = 0$ or $\rho_j = 0$ to ensure the analyzed V_R and V_T always approach to zero toward the vortex center. In (6c), the Gaussian correlation function is extended periodically over the periodic domain of $-\pi/\Phi < \phi \leq \pi/\Phi$ in (6c). The reduced form of $C_2(\phi_i - \phi_j)$ in the last step of (6c) will be used with $\Phi = 1$. The formulations in (6) indicate that $C(\rho_i, \rho_j, \phi_i - \phi_j)$ is nearly homogeneous and

isotropic when $\rho_i > 1$ and $\rho_j > 1$ and becomes virtually homogeneous and isotropic when $\rho_i > 2$ and $\rho_j > 2$ in the transformed (ρ, ϕ) -space but is stretched in the azimuthal direction along the curved vortex flow in the original (x, y) -space.

Since the radial de-correlation length equals to 1 in ρ , the associated radial de-correlation length in the physical space can be estimated by $R_c \exp[l(\rho + 1/2)] - R_c \exp[l(\rho - 1/2)] = 2R_c \sinh(l/2)$. The radial de-correlation length in the physical space is thus a linear function of R , which is similar to the azimuthal de-correlation arc length, that is, ΦR as a linear function of R . With this property, the correlation structure defined by $C(\rho_i, \rho_j, \phi_i - \phi_j)$ as a function of \mathbf{x}_j for given \mathbf{x}_i is nearly invariant in shape but its size increases linearly with $|\mathbf{x}_i|$. When $|\mathbf{x}_i|$ reaches the boundaries of the nested domain (of $2L \times 2L$ with $L = 10$ km) the radial de-correlation length in the physical space increases to $2L \sinh(l/2) \approx 6$ km (for $l = 1/2$) and the azimuthal de-correlation arc length increases to $\Phi L = 10$ km (for $\Phi = 1$). These increased de-correlation lengths around the nested domain boundaries should be compatible with the error de-correlation length for the mesoscale background flow outside the nested domain.

c. Square root of background error covariance

The square root of the background error covariance matrix can be derived analytically as shown below. First, one can verify that the correlation functions defined in (6b) and (6c) can be expressed by the following integrals:

$$C_1(\rho_i, \rho_j) = \int_0^\infty P_1(\rho_i, \rho_s) P_1(\rho_s, \rho_j) d\rho_s, \quad (7a)$$

$$C_2(\phi_i - \phi_j) = \int_{-\pi}^\pi P_2(\phi_i - \phi_s) P_2(\phi_s - \phi_j) d\phi_s, \quad (7b)$$

$$P_1(\rho_i, \rho_s) = (2/\pi)^{1/4} \{ \exp[-(\rho_i - \rho_s)^2] - \exp[-(\rho_i + \rho_s)^2] \}, \quad (8a)$$

$$\begin{aligned} P_2(\phi) &= (2/\pi)^{1/4} A_0^{-1/2} \sum_n \exp[-(\phi - 2n\pi/\Phi)^2] \\ &\approx (2/\pi)^{1/4} \exp(-\phi^2) \text{ for } -\pi/\Phi \leq \phi \leq \pi/\Phi \text{ and } \Phi \leq 1. \end{aligned} \quad (8b)$$

The truncation error for the approximation in the last step of (8b) is within $\pm \exp(-\pi^2/\Phi^2)$, and $\exp(-\pi^2/\Phi^2) \ll 1$ for $\Phi \leq 1$.

For the wind analyses performed in this paper, the two correlated points \mathbf{x}_i and \mathbf{x}_j are confined within the range circle of $R = \sqrt{2}L$ that encircles the nested analysis domain, so ρ_i and ρ_j are confined between 0 and $\rho_{\max} = l^{-1} \ln(1 + \sqrt{2}L/R_c) = 5.435$ (for $L = 10$ km). Note that the integrand $P_1(\rho_i, \rho_s) P_1(\rho_s, \rho_j)$ in (7a) becomes negligibly small as $\rho_s > \rho_{\max} + 2$ for ρ_i and ρ_j confined between 0 and ρ_{\max} . This implies that the integration range in (7a) can be reduced from $0 \leq \rho_s < \infty$ to $0 \leq \rho_s \leq \rho_{\max} + 2$, so the integral in (7a) can be discretized into the following form:

$$C_1(\rho_i, \rho_j) \approx \sum_{s'} P_1(\rho_i, \rho_{s'}) P_1(\rho_{s'}, \rho_j) \Delta\rho = \sum_{s'} P_{1is'} P_{1s'j}, \quad (9)$$

where $P_{1is'} = P(\rho_i, \rho_{s'}) (\Delta\rho)^{1/2}$, $P_{1s'j} = P(\rho_{s'}, \rho_j) (\Delta\rho)^{1/2}$, $\Delta\rho$ is the grad spacing of discretized $\rho_{s'} = (s' + 1/2)\Delta\rho$, $\sum_{s'}$ denotes the summation over integer s' from 0 to $S = \text{Int}[(\rho_{\max} + 2)/\Delta\rho]$, and $\text{Int}[(\)]$ denotes the nearest integer of $(\)$. To adequately resolve $P_1(\rho_i, \rho_{s'})$, $\Delta\rho$ should not exceed 1/2.

Similarly, the convolution integral in (7b) can be discretized into the following form:

$$C_2(\phi_i - \phi_j) \approx \sum_{s'} P_{2is'} P_{2s'j}, \quad (10)$$

where $P_{2is'} \equiv P_2(\phi_i - s' \Delta \phi) (\Delta \phi)^{1/2}$, $P_{2s'j} \equiv P_2(s' \Delta \phi - \phi_j) (\Delta \phi)^{1/2}$, $\Delta \phi = \pi / (M \Phi)$ is the grad spacing for discretized $\phi_s = s' \Delta \phi$, and $\sum_{s'}$ denotes the summation over integer s' from 1 - M to M . To adequately resolve $P_2(\phi)$, $\Delta \phi$ should not exceed 1/2, so M must be larger than π / Φ . The truncated form of $P_2(\phi)$ at the last step of (8b) is used to compute $P_{2is'}$ and $P_{2s'j}$ for $\Phi = 1$.

Substituting (9) and (10) into (6a) gives

$$C(\rho_i, \rho_j, \phi_i - \phi_j) \approx \sum_{s'} \sum_{s''} P_{1is'} P_{1s''j} P_{2is'} P_{2s''j} = \sum_{s'} P_{is'} P_{s''j}, \quad (11a)$$

where $P_{is} \equiv P_{1is'} P_{2is''}$ and the index s counts through all the grid points of (s', s'') over the two-dimensional control-variable domain with $0 \leq s' \leq S$ and $1 - M \leq s'' \leq M$. The matrix form of (11a) is

$$\mathbf{C} = \mathbf{P} \mathbf{P}^T, \quad (11b)$$

where the ij^{th} element of \mathbf{C} is given by $C_1(\rho_i - \rho_j) C_2(\phi_i - \phi_j)$ with the index i (or j) counting through all the grid points over the two-dimensional analysis domain except for the central grid point (at the vortex center where Δu and Δv must be zero), and the is^{th} element of \mathbf{P} is given by $P_{is} = P_{1is'} P_{2is''} = P_1(\rho_i, \rho_s) P_2(\phi_i - \phi_s) (\Delta \rho \Delta \phi)^{1/2}$ with the index s counting through all the grid points of (s', s'') . As shown in (11b), \mathbf{P} is an analytically constructed square root of \mathbf{C} .

For the selected values of $l = 1/2$, $\Phi = 1$ and $R_c = 1$ km, the dimension of (s', s'') depends on $(\Delta \rho, \Delta \phi)$ – the grid resolutions of the control-variable domain. Clearly, choosing relatively large $(\Delta \rho, \Delta \phi)$ can reduce the dimension of (s', s'') and thus improve the computational efficiency. On the other hand, $\Delta \rho$ and $\Delta \phi$ should not exceed 1/2 in order to adequately resolve $P_1(\rho)$ and $P_2(\phi)$. As an optimal trade-off, we set $\Delta \rho = 1/2$ and $\Delta \phi = \pi / (9 \Phi) (< 1/2)$. This gives $S = 15$ and $M = 9$, so the dimension of (s', s'') is $16 \times 18 = 288$, and the dimension of matrix \mathbf{P} indexed by (s, i) is $288 \times [(2L/\Delta x + 1)^2 - 1]$, where Δx is the grid spacing for the analyzed fields in the nested domain excluding the grid point at the vortex center. With the above discretization, the correlation function constructed from the square root matrix \mathbf{P} by using (11) is almost identical to the original correlation function formulated in (6), and the maximum difference is well within 1%.

Substituting (11) into (5b) gives $\mathbf{B} = (\sigma_R^2 \mathbf{C}, \sigma_T^2 \mathbf{C})^{\text{diag}} = (\sigma_R \mathbf{P}, \sigma_T \mathbf{P})^{\text{diag}} (\sigma_R \mathbf{P}^T, \sigma_T \mathbf{P}^T)^{\text{diag}}$, so $\mathbf{B}^{1/2} \equiv (\sigma_R \mathbf{P}, \sigma_T \mathbf{P})^{\text{diag}}$ is a root square of \mathbf{B} satisfying $\mathbf{B}^{1/2} \mathbf{B}^{T/2} = \mathbf{B}$. Substituting $\mathbf{a} = \mathbf{B}^{1/2} \mathbf{c}$ with $\mathbf{O} = \sigma_0^2 \mathbf{I}$ into (3) gives

$$J = |\mathbf{c}|^2 / 2 + |\mathbf{H}' \mathbf{c} - \mathbf{d} / \sigma_0|^2 / 2, \quad (12)$$

where $\mathbf{H}' = \sigma_0^{-1} \mathbf{H} \mathbf{B}^{1/2}$ is the σ_0 -scaled radial-velocity observation operator for the transformed control vector $\mathbf{c} \equiv (\mathbf{c}_R^T, \mathbf{c}_T^T)^T$, and the two components of the partitioned state vector $\mathbf{a} \equiv (\mathbf{a}_R^T, \mathbf{a}_T^T)^T$ are related to \mathbf{c}_R and \mathbf{c}_T by

$$\mathbf{a}_R = \sigma_R \mathbf{P} \mathbf{c}_R, \quad (13b)$$

$$\mathbf{a}_T = \sigma_T \mathbf{P} \mathbf{c}_T. \quad (13c)$$

Substituting (13) into (11) gives

$$\Delta u(\mathbf{x}_i) = \sigma_R \cos \beta_i \sum_s P_{is} c_{R_s} - \sigma_T \sin \beta_i \sum_s P_{is} c_{T_s}, \quad (14a)$$

$$\Delta v(\mathbf{x}_i) = \sigma_R \sin \beta_i \sum_s P_{is} c_{R_s} + \sigma_T \cos \beta_i \sum_s P_{is} c_{T_s}, \quad (14a)$$

where \mathbf{x}_i denotes the i^{th} grid point in the nested domain.

Substituting (14) into (2) gives

$$v_r(\mathbf{x}_i) = \sigma_R \sum_s R_{is} c_{R_s} + \sigma_T \sum_s T_{is} c_{T_s},$$

where \mathbf{x}_i denotes the i^{th} observation point over the nested domain, $R_{is} = \cos \theta_i \sin(\varphi_i + \beta_i) P_{is}$ and $T_{is} = \cos \theta_i \cos(\varphi_i + \beta_i) P_{is}$. Here, $\mathbf{H}' = \sigma_0^{-1} \mathbf{H} \mathbf{B}^{1/2}$ is derived analytically in the form of $\mathbf{H}' = (\sigma_R \mathbf{R}, \sigma_T \mathbf{T}) / \sigma_0$ with the is^{th} element of \mathbf{R} (or \mathbf{T}) given by R_{is} (or T_{is}). Note that \mathbf{x}_i can be any point in the continuous space of \mathbf{x} excluding the vortex center, so the analytical form of \mathbf{H}' can be applied to continuous observations to construct a more accurate integral-form observation operator.

Since the nested domain is small, \mathbf{c}_T and \mathbf{c}_R are constructed on a 16×18 uniform (ρ, ϕ) -grid with $\Delta \rho = 1/2$ to cover the range of $0 \leq \rho \leq \rho_{\text{max}} + 2$ and $\Delta \phi = \pi / (9 \Phi) (< 1/2)$ to cover the entire range of $-\pi / \Phi < \phi \leq \pi / \Phi$. In this case, although the observation space dimension can exceed 10^4 , the control-vector space dimension is merely $2 \times 16 \times 18 = 576$, so the preconditioned cost-function in (12) can be minimized efficiently by using the conjugate-gradient descent algorithm. Substituting the minimizer \mathbf{c} back into (14) gives the analyzed vortex wind field $(\Delta V_R, \Delta V_T)$. In particular, the vortex analysis takes less than 6 seconds of Central Processing Unit (CPU) time.

For the illustrative examples presented in the next section, the error standard deviation for the dealiased radial-velocity observations is set to $\sigma_0 = 2 \text{ ms}^{-1}$ in the cost-function, and this setting is the same as that used to estimate the super-observation error standard deviation in section 3.3 of Xu et al. (2015a). Since the background wind (u^b, v^b) is uniform in the nested analysis domain, the background wind errors can be as large as the true vortex winds. The maximum of the vortex winds estimated from $v_r^0(r, \varphi)$ is $V_M \approx 45 \text{ ms}^{-1}$, so $\sigma_T = \sigma_R = 20 \text{ ms}^{-1}$ can be used for constructing the preconditioned cost-function in (12).

3. Examples

The method has been applied in a stand-alone fashion to the KTLX radial-velocity scans of the tornadic mesocyclone and its produced EF5 tornado that struck the cities of Newcastle and Moore, Oklahoma in the afternoon (local time between 2:45pm and 3:35pm) on 20 May 2013. As an example, three sequentially analyzed vortex wind fields are plotted in Fig. 1 by the color-scaled arrows superimposed on the radial-velocity innovation images from KTLX radar on 0.5° tilt (around $z = 0.67$ km) for three consecutive volume scans from 2008:42 to 2017:15 UTC 20 May 2013. The maximum tangential velocity and its radial distance from the vortex center for the vortex wind field in each panel of Fig. 7 are close to those ($V_M \approx 45 \text{ ms}^{-1}$ and $R_M \approx 0.5$ km) estimated directly from the KTLX radial-velocity observations.

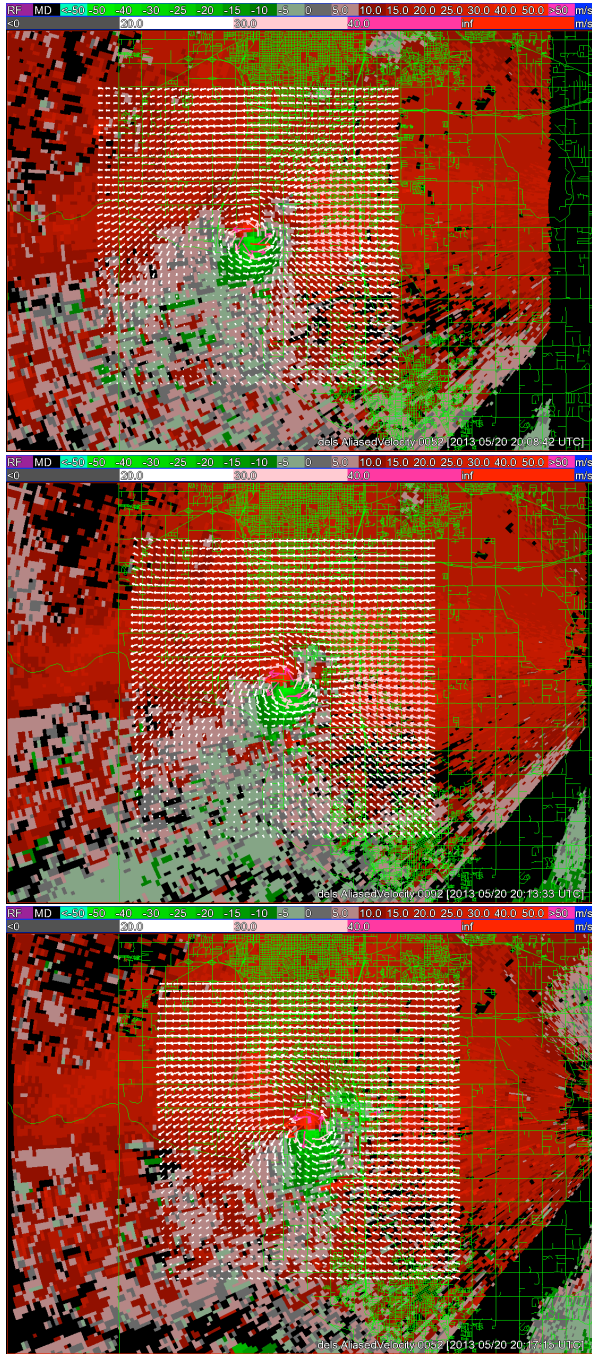


Fig. 1. Analyzed vortex wind fields plotted by color-scaled arrows superimposed on the images of radial-velocity innovation v_r^i ($= v_r^o - v_r^b$) from KTLX radar on 0.5° tilt (around $z = 0.67$ km) for three consecutive volume scans of the tornadic mesocyclone from 2008:42 to 2017:15 UTC 20 May 2013. The thin green lines in each panel show the county boundaries and streets of city Moore. The KTLX radar is located at about $(x, y) = (29, -2)$ km outside the analysis domain in the first panel.

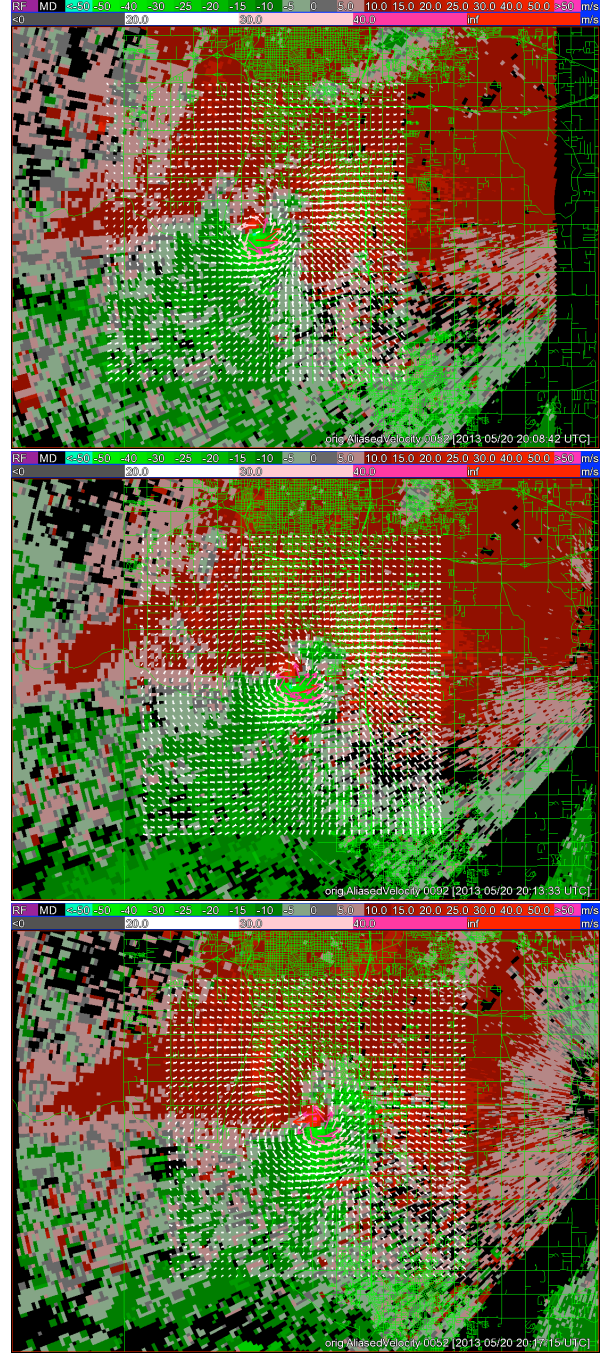


Fig. 2. As in Fig. 1 but for the analyzed total wind fields superimposed on the images of dealiased radial-velocity observations v_r^o from KTLX radar on 0.5° tilt.

The total wind fields [that is, the vortex wind fields in Fig. 1 plus their respective background winds (u^b, v^b)] are shown in Fig. 2 by the color-scaled arrows superimposed on the images of dealiased radial-velocity observations v_r^o from KTLX radar on 0.5° tilt. As shown, the winds were strongest in a small area immediately to south and southeast of the vortex center in each panel and this high-wind area was moving with the tornadic mesocyclone toward city Moore.

The above results indicate that the total wind fields produced by the method can be very useful for nowcasting the tornadic mesocyclone and associated high-wind areas. The consistency and stability of the method have been further examined and well verified by applying the method to the entire time series of consecutive data volumes (from 1951:42 to 2030:00 UTC) for the above case, and the detailed results are shown by the movies presented at the conference and posted online at the AMS web site.

4. Conclusions

This paper reports a recently developed new method for analyzing the vortex wind fields from radar observed mesocyclones. The method is shown to be computational very efficiently and it can retrieve the vortex part of the mesocyclone winds from single-Doppler observations. These are the strengths of the method. The method is expected to work best when the mesocyclone is intense and not too far (within 100 km) from the radar, and this is another strength of the method. On the other hand, the method may not work well when the mesocyclone is small and far from the radar where the radar beams become wider than the vortex core diameter. The effectiveness and performance of the method are demonstrated by examples of analyzed vortex wind fields and total wind fields for the Oklahoma tornadic mesocyclones observed by the KTLX radar on 20 May 2013. With a reliably estimated background wind, the total wind field produced by the method can be very useful for nowcasting tornadic mesocyclones and associated high-wind areas (see Fig. 2).

The method can be also incorporated into the existing radar wind analysis system (RWAS, Xu et al. 2015a) as an additional (fourth) step of targeted fine-scale analysis after the third step is performed in the RWAS. This application and related performances are presented in Xu et al. (2015b). The method is currently extended to analyze three-dimensional vortex winds in the Cartesian coordinates from either single-Doppler or multi-Doppler scans of mesocyclones with the background wind error correction functions formulated in a slantwise cylindrical coordinate system co-centered with the mesocyclone at each vertical level. The progress and preliminary results in this direction can be found from the ppt file presented at the conference and posted online at the AMS web site.

Acknowledgments

The research work was supported by the ONR Grant N000141410281 to the University of Oklahoma (OU). Funding was also provided to CIMMS by NOAA/Office of Oceanic and Atmospheric Research under NOAA-OU Cooperative Agreement #NA17RJ1227, U.S. Department of Commerce.

REFERENCES

Gao, J., T. M. Smith, D. J. Stensrud, C. Fu, K. Calhoun, K. L. Mnaross, J. Brogden, V. Lakshmanan, Y. Wang, K. W. Thomas, K. Brewster, and M. Xue, 2013: A realtime weather-adaptive 3DVAR analysis system for severe weather detections and warnings. *Wea. Forecasting*, **28**, 727–745.

Liu, S., M. Xue, and Q. Xu, 2007: Using wavelet analysis to detect tornadoes from doppler radar radial-velocity observations. *J. Atmos. Oceanic Technol.*, **24**, 344–359.

Miller, M. L., V. Lakshmanan, and T. M. Smith, 2013: An automated method for depicting mesocyclone paths and intensities. *Wea. Forecasting*, **28**, 570–585.

Newman, J. F., V. Lakshmanan, P. L. Heinselman, M. B. Richman, and T. M. Smith, 2013: Range-correcting azimuthal shear in Doppler radar data. *Wea. Forecasting*, **28**, 194–211.

Smith, T. M., and K. L. Elmore, 2004: The use of radial velocity derivatives to diagnose rotation and divergence. Preprints, *11th Conf. on Aviation, Range and Aerospace*, Hyannis, MA, Amer. Meteor. Soc., P5.6.

Stumpf, G. J., A. Witt, E. D. Mitchell, P. L. Spencer, J. T. Johnson, M. D. Eilts, K. W. Thomas, and D. W. Burgess, 1998: The National Severe Storms Laboratory mesocyclone detection algorithm for the WSR-88D. *Wea. Forecasting*, **13**, 304–326.

Xu, Q., K. Nai, S. Liu, C. Karstens, T. Smith and Q. Zhao, 2013: Improved Doppler velocity dealiasing for radar data assimilation and storm-scale vortex detection. *Advances in Meteorology*. vol. **2013**, Article ID 562386, 10 pages.

Xu, Q., L. Wei, K. Nai, S. Liu, R. M. Rabin, and Q. Zhao, 2015a: A radar wind analysis system for nowcast applications. *Advances in Meteorology*. vol. **2015**, Article ID 264515, 13 pages.

Xu, Q., L. Wei and K. Nai, 2015b: Analyzing vortex winds in radar observed tornadic mesocyclones for nowcast applications. *Wea. and Forecasting*, (in press).